THE JOURNAL OF PHYSICAL CHEMISTRY A

Article

pubs.acs.org/JPCA

Precipitates of Al(III), Sc(III), and La(III) at the Muscovite–Water Interface

Sarah A. Saslow Gomez and Franz M. Geiger*

Department of Chemistry, Northwestern University, 2145 Sheridan Road, Evanston, Illinois 60208, United States

Supporting Information

ABSTRACT: The interaction of Al(III), Sc(III), and La(III) with muscovite–water interfaces was studied at pH 4 and 10 mM NaCl using second harmonic generation (SHG) and X-ray photoelectron spectroscopy (XPS). SHG data for Sc(III) and La(III) suggest complete and/or partial irreversible adsorption that is attributed by XPS to the growth of Sc(III) and La(III) hydroxides/oxides on the muscovite surface. Al(III) adsorption appears to coincide with the growth of gibbsite ($Al(OH)_3$) deposits on the muscovite surface, as indicated by the magnitude of the interfacial potential computed from the SHG data. This interpretation of the data is consistent with previous studies reporting the epitaxial growth of gibbsite on the muscovite surface under similar conditions. The implication of our findings is that the surface charge density of mica may change (and in the case of Al(III), even flip sign from negative (mica) to positive (gibbsite)) when Al(III), Sc(III), or La(III) is present in aqueous phases in contact with heterogeneous geochemical media rich in mica-class minerals, even at subsaturation conditions.

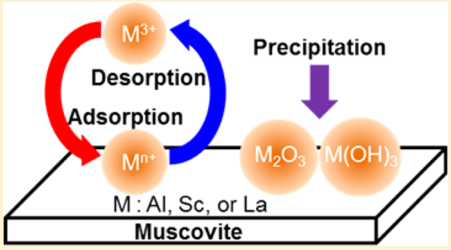

1. INTRODUCTION

The interactions of metal contaminants at the mineral–water interface largely dictate their mobility and transport in groundwater systems.[1−3] Important interactions include adsorption/desorption processes, as well as the precipitation of a solution component. Precipitation below bulk saturation in the presence of a surface has been shown to occur in numerous mineral–water systems.[1,2] A possible consequence of precipitation reactions at the mineral–water interface can be a change in solute mobility due to possible changes in interfacial charge densities and thereby interfacial potentials. This situation may arise when an amphoteric oxide precipitates on top of a mineral that is not amphoteric, such as hydroxide formation on mica-class minerals, which is the focus of this present study.

While gaining a molecular understanding of surface processes occurring at mineral–aqueous interfaces appears necessary for predicting and controlling geochemical processes,[4,5] doing so is difficult because of the limited applicability of most surface science techniques to probe solid–aqueous interfaces directly. Here, we probe the interfacial interactions—specifically the possibility for precipitation—of trivalent metal ions at the muscovite–water interface using the interface-specific technique second harmonic generation (SHG) paired with offline surface analytics, including X-ray photoelectron spectroscopy (XPS). Mica-class minerals are a common constituent of soils and are known for their highly reactive surface sites and high cation exchange capacities.[6,7] These materials are prone to undergo adsorption/desorption processes and can facilitate the precipitation of secondary minerals that can consequently increase or decrease the mobility of metal ions.[1,8] Here, we use the common soil constituent muscovite (herein also referred to as mica), $KAl_2(AlSi_3O_{10})(OH,F)_2$, known for its near-perfect cleavage and minimal swelling when exposed to aqueous solutions.[7,9] Al^{3+} substitution for Si^{4+} atoms results in an inherent negative charge within the crystal lattice that is balanced by counterions, typically K^+, between the tetrahedral–octahedral–tetrahedral (T–O–T) layers.[10] Due to the role of Al^{3+} in the mineral structure of muscovite and the relatively straightforward speciation of Al^{3+} in solution, we chose to study the interactions of Al^{3+} ions with the muscovite surface. Furthermore, by using SHG, we overcome the common experimental challenge of distinguishing Al(III) ions interacting at the interface and the Al-containing mineral. In addition to studying the interactions of Al(III) with the muscovite–water interface, the rare earth elements (REEs) La(III) and Sc(III) were also investigated due to the rising concern about their environmental impacts in the form of electronic waste.[11−15] As we discuss further below, only a few research studies have investigated Al(III) adsorption to muscovite to date.[2,16] Furthermore, to our knowledge, this work is the first to investigate La(III) and Sc(III) interactions at the muscovite–water interface.

The methods most commonly used to study the adsorption/desorption properties of metal ions at the mineral–water interface include batch studies,[17] X-ray techniques,[16,18,19] atomic force microscopy (AFM),[2] and theoretical modeling.[20,21] Generally, a combination of techniques is necessary for elucidating ion interactions directly at mineral–water interfaces. By pairing standard surface analytical tools with SHG, we make a step toward this goal by probing the mica–water interface

Received: June 24, 2014
Revised: October 17, 2014
Published: October 21, 2014

directly while monitoring ion interactions as a function of interfacial potential under environmentally relevant electrolyte concentrations and pH conditions. Results obtained using SHG are acquired under aqueous flow conditions, in real time, and with submicromolar sensitivity to which the aforementioned theoretical and analytical techniques can be readily compared.[22] XPS is also used to analyze the mica surface for the precipitation of secondary mineral phases in addition to Raman spectroscopy and the complementary surface analytical techniques grazing incidence angle X-ray diffraction (GIAXRD), scanning electron microscopy (SEM), and energy dispersive X-ray spectroscopy (EDS).

2. EXPERIMENTAL METHODS

A. Sample Preparation. For all experiments, V1-quality muscovite disks were purchased from Ted Pella, Inc. All muscovite samples were approximately 0.21 mm thick and 20 mm in diameter. The day prior to experimentation, muscovite disks were sonicated in methanol for 6 min, dried in a drying oven (110 °C) for 10 min, and then plasma cleaned for 30 s at the highest setting (Harrick Plasma, Plasma Cleaner PDC-32G). The disk was then soaked overnight in a 10 mM NaCl (VWR, 99.0%) solution made with Millipore water (18 MΩ). Additionally, a fused silica hemisphere (ISP Optics, 1 in. diameter), used in the SHG experiments, was surface treated with NoChromix (Godax Laboratories) for 1 h, followed by the methanol and plasma cleaning procedure previously described. A 20 L carboy was filled with Millipore (18 MΩ) water and allowed to equilibrate with atmospheric CO_2 overnight. Finally, just before experimentation, the 20 L carboy was adjusted to 10 mM NaCl (VWR, 99.0%) and then used to prepare NaOH (Sigma-Aldrich, 99.99%) and HCl (EMD ACS grade) solutions of ∼1 M, used to regulate pH conditions throughout the duration of the experiment and to prepare 10 mM solutions of Al(III), La(III), and Sc(III) using $AlCl_3{\cdot}6H_2O$ (Alfa Aesar, 99.995%), $LaCl_3{\cdot}7H_2O$ (Aldrich, 99.999%), and $ScCl_3{\cdot}6H_2O$ (Alfa Aesar, 99.99%), respectively.

B. Laser and Flow System. A detailed description of our laser setup can be found in our previous publications.[23−27] Briefly, all SHG experiments were carried out using a regeneratively amplified Ti:sapphire laser (Hurricane, Spectra Physics, 120 fs pulse) pumping an optical parametric amplifier (OPA-CF, Spectra Physics, 1 kHz repetition rate) tuned to produce 680 ± 5 nm light, unless otherwise specified. The OPA output energy was attenuated to 0.40 ± 0.02 μJ using a variable density filter, then passed through a half-wave plate selecting for p-polarization, and focused at the mica−water interface at an incident angle of 60°, just below total internal reflection. The SHG produced was then separated from the fundamental (ω) using a Schott filter, directed through a monochromator set to the SHG wavelength (340 nm), and finally into a photomultiplier tube (Pacific Instruments). A gated single-photon counter (Stanford Research Systems SR400) was then used to record the SHG photons collected, after preamplification, per second.

All SHG experiments were conducted in triplicate to assess reproducibility. Using the Teflon flow cell design described in our previous work,[23,25−28] experiments were carried out under environmentally relevant flow conditions (mean stream velocity ≈ 1 cm/sec,[29] unless otherwise noted) using a dual pump flow system for switching between background electrolyte and metal solution reservoirs. The mica disk was clamped atop the flow cell between a Viton O-ring and the fused-silica hemisphere, forming a leak-tight seal. A ring of 10 mM NaCl solution was placed around the hemisphere and disk to saturate the mica interlayers. Additional 10 mM NaCl solution was added as necessary throughout the experiment when evaporation occurred. The ring of electrolyte solution proved critical to the stability of the SHG responses, as illustrated in Figures S3 and S4 in the Supporting Information. In the absence of the 10 mM NaCl ring, signal fluctuations of varying amplitude and duration were observed over the course of an experiment. The 10 mM NaCl was used regardless of the experimental background concentrations as fluctuations were observed at concentrations lower than 10 mM NaCl as well. Once the mica sample was set, 1 L of background electrolyte solution was flowed through both reservoirs and flow tubes to rinse the system. A conductivity meter (Fisher Traceable Conductivity and TDS meter, Fisher Scientific) was used to verify the concentration of NaCl in all electrolyte solutions.

C. Surface Characterization. For bulk elemental analysis of the mica surface, XPS experiments were performed using a Thermo Scientific ESCALAB 250Xi spectrometer equipped with a monochromatic Al Kα X-ray source and flood gun for charge compensation. Binding energies were corrected by reference to the C 1s peak at 285 eV. Raman spectroscopy, GIAXRD, SEM, and EDS were also used. Details regarding supporting instrumentation are provided in the Supporting Information.

D. SHG Background. We use SHG, specifically the nonresonant $\chi^{(3)}$ technique, to study the electrostatic properties of the mica−water interface as a function of metal concentration.[23,24,30,31] The SHG response depends on the static interfacial potential, Φ_0, present at the charged interface, according to

$$\sqrt{I_{SHG}} \propto E_{SHG} \propto \chi^2 E_\omega E_\omega + \chi^3 E_\omega E_\omega \Phi_0 \quad (1)$$

Here, χ^2 and χ^3 are the second- and third-order nonlinear susceptibility tensors, respectively, E_ω is the incident electric field, E_{SHG} is the generated second-order electric field, and I_{SHG} is the SHG signal intensity. Intuitively, one can think of this method as an optical voltmeter, and the assumptions, capabilities, and limitations of the method have been described in our earlier work.[32,33]

By using the Gouy−Chapman equation, we can write the interfacial potential as a function of the surface charge density, σ, background electrolyte concentration, C_{elec}, and metal concentration, M, as follows[4,5,34]

$$\Phi_0 = \frac{2k_BT}{ze}\sinh^{-1}\left(\sigma\sqrt{\frac{\pi}{2\varepsilon\varepsilon_0 T(C_{elec}+M)}}\right) \quad (2)$$

Here, k_B is the Boltzmann constant, T is temperature, z is the charge on the electrolyte ion, e is the elemental charge, ε is the dielectric constant of water at 25 °C, and ε_0 is the permittivity in a vacuum. Equation 2 shows that an increase in the bulk electrolyte concentration will result in a proportional change in SHG signal intensity.

In instances when metal ions are present, the net surface charge density, σ, can be written as the sum of the initial surface charge density present at the mineral surface in the absence of metal adsorbates, σ_0, and the interfacial charge density due to metal adsorbates at maximum coverage, σ_m, scaled by the surface coverage modeled by the Langmuir adsorption model.[25,27] Combined with the expression for the interfacial

dx.doi.org/10.1021/jp506283y | J. Phys. Chem. A 2014, 118, 10974−10981

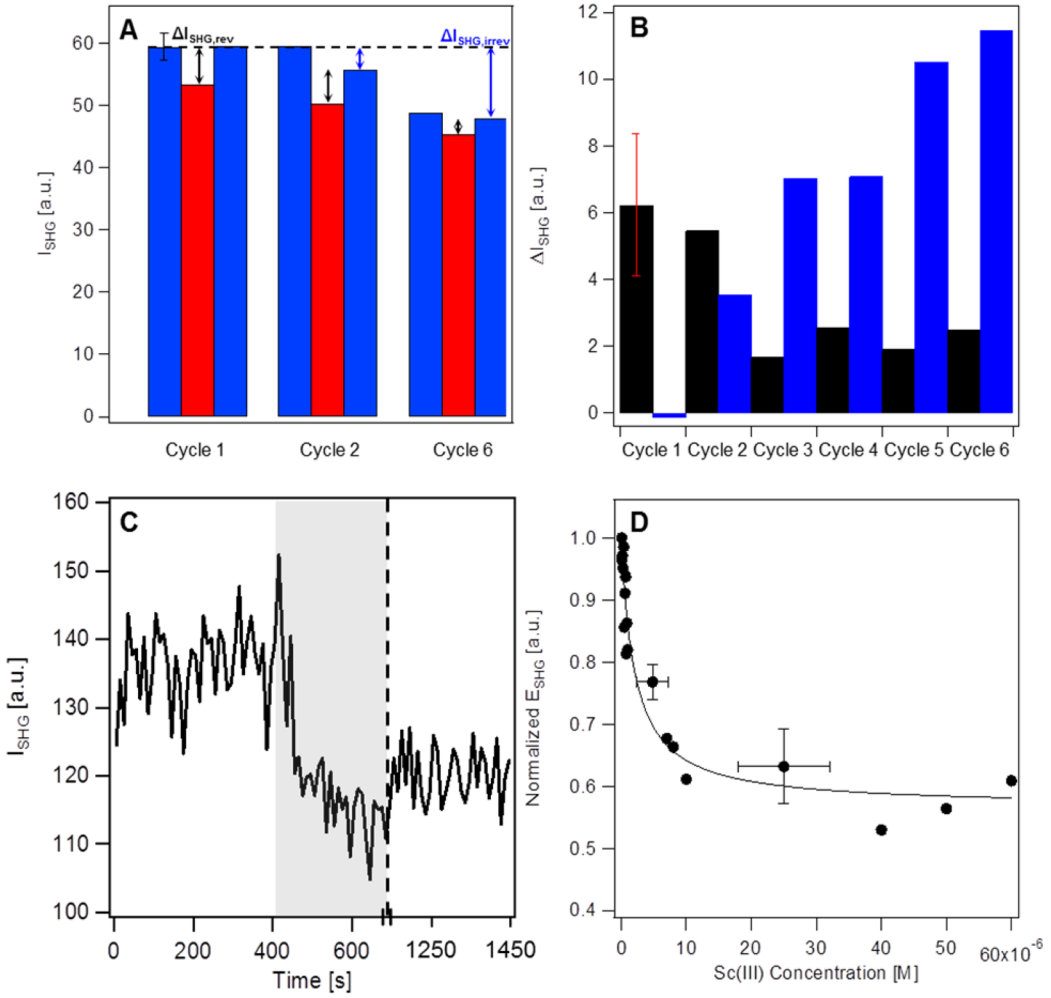

Figure 1. (A) Bar graph showing the average SHG signal intensity for the first, second, and sixth cycles of 0.25 mM La(III). Blue and red bars indicate 10 mM NaCl background solution and La(III) solutions, respectively. Arrows show the change in intensity for both the reversible ($\Delta I_{SHG,rev}$, black) and irreversible ($\Delta I_{SHG,irrev}$, blue) components. The error range for SHG signal intensity is indicated atop the first rinse of 10 mM NaCl in cycle 1. (B) Irreversible and reversible SHG components as a function of cycle of 0.25 mM La(III). (C) Sc(III) adsorption is largely irreversible after exposure to 0.7 μM Sc(III) and being rinsed with 10 mM NaCl. The gray shaded region highlights the duration of time that Sc(III) was being flowed across the mica surface. The dashed line indicates a 350 s period of time removed from the trace where the laser power briefly increased. (D) Sc(III) irreversible adsorption isotherm. E_{SHG} values were calculated by taking the square of the average SHG signal intensity for a given metal concentration and dividing by the square of the average SHG signal intensity of the background electrolyte baseline established in the first 300 s of the experiment. Error bars are indicative of averaged points. The black line serves as a guide to the eye.

potential in eq 2, we model the observed SHG signal intensity as a function of metal ion concentration as follows

$$\sqrt{I_{SHG}} = A + B \sinh^{-1}\left[\left(\sigma_0 + \sigma_m\left(\frac{K_{ads}[M]}{1 + K_{ads}[M]}\right)\right) \times \sqrt{\frac{\pi}{2\varepsilon\varepsilon_0 T(C_{elec} + M)}}\right] \quad (3)$$

where A and B are composed of constants from eqs 1 and 2, including nonlinear susceptibility tensors χ^2 and χ^3 and the incident electric field E_ω, which have been shown to remain constant over the ionic strengths used in this work,[35] and K_{ads} is the equilibrium binding constant of the metal analyte. The initial surface charge density, σ_o, of the mica surface under the experimental conditions used in this work (pH 4) was experimentally determined to be −0.002(2) C m^{-2},[22] which agrees with results from a recent computational study by Teich-McGoldrick et al.[36] The nature of the initial surface charge density of the muscovite surface is explained in detail in the Supporting Information.

3. RESULTS AND DISCUSSION

A. Adsorption of Lanthanum and Scandium. The interactions of La(III) and Sc(III) with the mica basal surface were investigated using SHG by collecting adsorption/desorption isotherms via the dual pump system described previously. To start, 10 mM NaCl, adjusted to pH 4, was flowed over the mica surface and allowed to equilibrate for ∼5 min, and then, the SHG signal response was collected for a minimum of 300 s. With an SHG signal baseline established, the aqueous flow was switched to draw from the reservoir containing a metal solution of known concentration made from the same background salt solution and adjusted to pH 4. According to eq 3, a decrease in interfacial potential due to the adsorption of metal ions at the surface will result in a proportional change in the SHG signal intensity. Upon observation of this change, the SHG signal intensity was

dx.doi.org/10.1021/jp506283y | J. Phys. Chem. A 2014, 118, 10974−10981

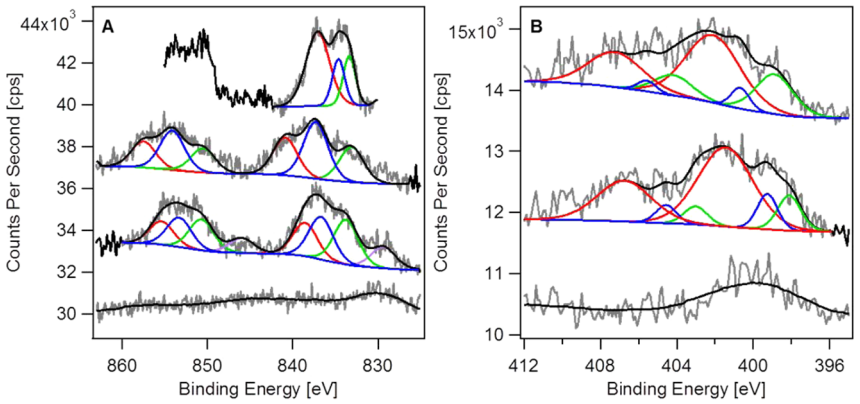

Figure 2. (A) XPS spectra of La(III) deposits that formed on the mica surface during SHG analysis. Raw spectra are shown in gray, and the peak fitting envelope is in black. The middle traces are from two different areas of the same sample, and the top trace is from a second sample. The bottom trace is the clean mica surface, and the black line is a boxcar trace. Fitted peak positions for La $3d_{5/2}$ and La $3d_{3/2}$ (green), as well as their respective bonding (red) and antibonding (blue) peaks, are also shown. The purple peaks are predicted to be La(III) satellite peaks. Spectra have been offset for clarity. (B) XPS spectra of Sc(III) deposits that formed on the mica surface while simulating SHG analysis. Two areas were analyzed on the sample; raw spectra are shown in gray, and the peak fitting envelope is in black. The bottom trace is the clean mica surface, and the black line is a boxcar trace. Fitted Sc $2p_{3/2}$ and Sc $2p_{1/2}$ peak positions for Sc(0), Sc_2O_3, and ScOOH are shown in green, blue, and red, respectively.

collected for an additional 300 s. Finally, the solution was switched back to the background salt solution to test for reversibility, indicated by a return of the SHG signal intensity to that of the baseline established at the start of the experiment. This process, herein also referred to as an "on-off" trace or experiment, was repeated while sequentially increasing the metal concentration. The results for two different phenomena observed for La(III) and Sc(III) are described below.

1. La(III). La(III) has a large ionic radius and a tendency to form chloride complexes at the silica surface that reduce its charge state;[37] therefore, it was anticipated that La(III) would weakly adsorb and readily desorb to and from the mica surface. Using the experimental procedure described above, adsorption isotherms were collected; however, a single La(III) concentration of 0.25 mM was used in several sequential on−off experiments. The first exposure of La(III) to the mica surface exhibited complete reversibility upon rinsing with the background electrolyte solution (Figure 1A); however, over the duration of the experiment, we found that the extent of reversibility decreased until no net change in SHG signal intensity between the background electrolyte solution and the La(III) solution was observed. We note here that while La(III) concentrations as low as 0.1 μM were also investigated, the dynamic range in SHG signal intensity is significantly larger at higher La(III) concentrations and best suited for this segment of our investigation. La(III) interactions with the muscovite−water interface are summarized for the micromolar regime in the Supporting Information.

On the basis of these observations, we hypothesize that with repeated exposure to La(III) ions in solution, desorption becomes less and less favorable until the mica surface is saturated with La(III), at which point no more adsorption/desorption behavior is observed. This trend in decreasing reversibility is similar to that observed in our previous work studying Cr(III) interactions with hematite surfaces.[38] Adopting the analysis established therein, the reversible and irreversible adsorption components for sequential La(III) cycles were calculated using the following equations (Figure 1A)

$$\Delta I_{SHG,rev} = I_{SHG,water} - I_{SHG,La(III)} \quad (4)$$

$$\Delta I_{SHG,irrev} = I_{SHG,baseline} - I_{SHG,water} \quad (5)$$

Here, $I_{SHG,water}$ is the SHG signal intensity after La(III) is rinsed from the mica surface with 10 mM NaCl, $I_{SHG,La(III)}$ is the SHG signal intensity while the mica surface is exposed to La(III), and $I_{SHG,baseline}$ is the SHG signal intensity of the baseline established from the background electrolyte at the start of the experiment. As illustrated in Figure 1B, with each subsequent exposure of La(III), the reversible and irreversible components decrease and increase, respectively, supporting our hypothesis that La(III) desorption from the mica surface becomes less favorable with repeated exposure to La(III) ions in solution. This is likely a due to the precipitation of La(III) deposits on the muscovite surface, as evidenced by XPS (vide infra).

2. Sc(III). Compared to La(III), Sc(III) is significantly smaller in size, has a larger charge to volume ratio and a larger hydration enthalpy.[39] On the basis of these bulk solution properties, we expect Sc(III) to adsorb closer to the muscovite surface and to interact more strongly with it if adsorption were to be electrostatically driven. As exemplified in Figure 1C, the observed SHG signal intensity decreases with increasing Sc(III) concentration; however, minimal reversibility is observed upon flushing the mica surface with background electrolyte. The isotherm shown in Figure 1D shows that with increasing Sc(III) concentration, there is a significant decrease in E_{SHG}. Because the adsorption process is shown to be largely irreversible, we further investigated whether Sc(III) deposits could be formed on the surface as well, just like in the case of La(III) (vide infra).

B. Surface Characterization and Analysis of Lanthanum and Scandium Deposits. The detection, characterization, and analysis of La(III) and Sc(III) deposits formed on the mica surface were accomplished using XPS because this technique was shown to identify the chemical nature of the Sc(III) and La(III) deposits with unmatched sensitivity compared to the other techniques tested in our work. The XPS results and the information that they provide regarding the interactions of trivalent metal cations with the mica surface are described below. Additional XPS scans as well as results from the additional techniques used to analyze the mica surface,

dx.doi.org/10.1021/jp506283y | J. Phys. Chem. A 2014, 118, 10974−10981

Table 1. Atomic % of Sc(III) and/or La(III) Deposits Detected by XPS on Mica Substrates

duration of soak		1 day			6 days			10 days		
metal(III)		Sc	La	Sc, La	Sc	La	Sc, La	Sc	La	Sc, La
solution concentration		1 mM	1 mM	both 1 mM	1 mM	1 mM	both 1 mM	1 mM	1 mM	both 1 mM
total atom %	Sc	0.76		1.12	1.23		0.55	1.26		0.9
	Sc(0)	0.14		0.35	0.08		0.04	0.09		0.15
	Sc_2O_3	0.3		0.15	0.56		0.16	0.75		0.45
	ScOOH	0.32		0.62	0.59		0.33	0.42		0.3
total atom %	La(III)		0.26	–		0.25	0.08		–	0.05
	La_2O_3 or $La(OH)_3$[a]		$La(OH)_3$	–		$La(OH)_3$	$La(OH)_3$		–	$La(OH)_3$

[a]The La(III) deposit present on the surface predicted based on peak positions is provided in the Supporting Information.

including Raman spectroscopy and GIAXRD, are provided in the Supporting Information.

1. La(III). The first La(III)-exposed mica sample analyzed by XPS after completion of an SHG experiment (top trace in Figure 2A) was found to exhibit strong spectral peaks resolved at binding energies associated with the La $3d_{5/2}$ and $3d_{3/2}$ photoelectrons, in addition to their associated bonding and antibonding satellite peaks.[18] To test the reproducibility of these results, a second mica disk was analyzed at two different surface locations by XPS after exposure to La(III) during an experiment simulating the conditions used during SHG analysis (two middle traces, Figure 2A). Similar results were obtained, but with less spectral resolution when compared to the first sample.

To determine the chemical composition of the deposits forming on the mica surface, we reference spectra published by Sunding et al.[18] yet caution that their investigation focused on La(III) hydroxide and oxide powders. A summary of the La $3d_{5/2}$ and $3d_{3/2}$ main peak positions and their satellites, for La_2O_3 or $La(OH)_3$, are provided in Table S2 in the Supporting Information. According to their work, the relative height (or intensity) ratio for the La_2O_3 $3d_{3/2}$ peak and its bonding satellite is approximately 1:1, and for the La_2O_3 $3d_{5/2}$ peak, it is slightly lower in intensity than its bonding satellite.[18] Additionally, the intensity of the $La(OH)_3$ 3d peak relative to its bonding satellite peak is slightly greater for the La $3d_{3/2}$ and La $3d_{5/2}$ transitions.[20] The intensity ratios in our XPS spectra therefore suggest that La_2O_3 is formed on the mica surface over the duration of the SHG adsorption experiments. Yet, we caution that the binding energies obtained from spectral fits (see Supporting Information) were inconclusive regarding the chemical state of the La(III) deposits present.

2. Sc(III). In Figure 2B, we show the XPS spectra for two different areas analyzed for Sc(III) on the same mica disk. As reported by Biesinger et al., the Sc $2p_{3/2}$ binding energies for Sc(0), Sc_2O_3, and ScOOH arise at 398.45, 401.71, and 402.87 eV, respectively.[19] Furthermore, Sc $2p_{1/2}$ peaks should be observable at around 403.19, 406.16, and 407.45 eV for Sc(0), Sc_2O_3, and ScOOH, respectively.[19] As shown in Figure 2B, several of these peaks were resolved within the designated spectral region and clearly confirm the presence of Sc(III) hydroxide/oxide deposits on the mica surface. Differences in the relative peak positions and intensities when compared to those reported by Biesinger et al. are attributed to differences in sample preparation.

C. Lanthanum and Scandium Deposit Formation on Mica after Extended Exposure. Further investigation into the time dependence on the formation of La(III) and Sc(III) deposits on the muscovite surface were conducted by soaking nine clean mica disks in solutions of 1 mM Sc(III), 1 mM La(III), or a solution containing both 1 mM Sc(III) and La(III) for 1, 6, and 10 days. Solutions were prepared in the presence of 10 mM NaCl and pH adjusted using 1 M HCl to pH 4. After soaking, the samples were rinsed with Millipore (18Ω) water, dried with N_2 gas, and analyzed by XPS. Using the Thermo Avantage software on the workstation of the XPS instrument, the presence of Sc(III) and/or La(III) on the muscovite surface was quantified by atomic percent. These results are summarized in Table 1, with additional spectra and peak analysis provided in the Supporting Information. XPS imaging and SEM/EDS results are also provided in the Supporting Information. Compared to XPS spectroscopy, XPS and EDS imaging techniques were significantly less sensitive and could not be adequately compared to the quantitative results provided in Table 1.

1. 1 mM La(III). For the 1 and 6 day exposures, 0.26 atomic percent (atom %) and 0.25 atom % were detected, respectively, whereas no La(III) deposits were detected for the sample analyzed after 10 days of La(III) exposure. Close examination of the fitted peak positions and relative separations, provided in the Supporting Information, suggests that the deposits formed are $La(OH)_3$, as opposed to the La_2O_3 putatively identified from the peak intensity ratio assessment of the short exposure experiments discussed earlier.

2. 1 mM Sc(III). The amount of Sc(III) on the mica surface increased with increased exposure time from 0.76 to 1.23 and 1.26 atom % for the 1, 6, and 10 day soaking experiments, respectively. Using the software peak fitting function, contributions from Sc(0), Sc_2O_3, and ScOOH deposits were calculated. The data show that the signal appearing at the Sc(0) line decreases with increased exposure/soaking time, whereas the Sc_2O_3 and ScOOH contributions increase. We caution that due to the redox inactivity in our system, Sc(0) formation should not occur, and the signals at 398.45 and 403.19 eV could be due to different species, which are not yet identified. With lower exposure times, the amount of oxide and hydroxide present was approximately equal; however, the Sc_2O_3 contributions were considerably greater after 10 days of exposure (0.75 atom %) than the ScOOH contributions (0.42 atom %).

3. Competitive Binding of 1 mM La(III) and 1 mM Sc(III). When exposed to both La(III) and Sc(III), significantly less La(III) presence was detected on the muscovite surface when compared to the La(III)-only experiments described above, and Sc(III) was detected in varying amounts for each sample. No La(III) deposits were detected after 1 day of soaking, whereas the 1.12 atom % of Sc(III) detected was the most Sc(III) detected out of the 1, 6, and 10 day soaking study. For the 6 and 10 day exposures, trace amounts of La(III) were detected at 0.08 and 0.05 atom %, respectively. The variability in the

dx.doi.org/10.1021/jp506283y | J. Phys. Chem. A 2014, 118, 10974−10981

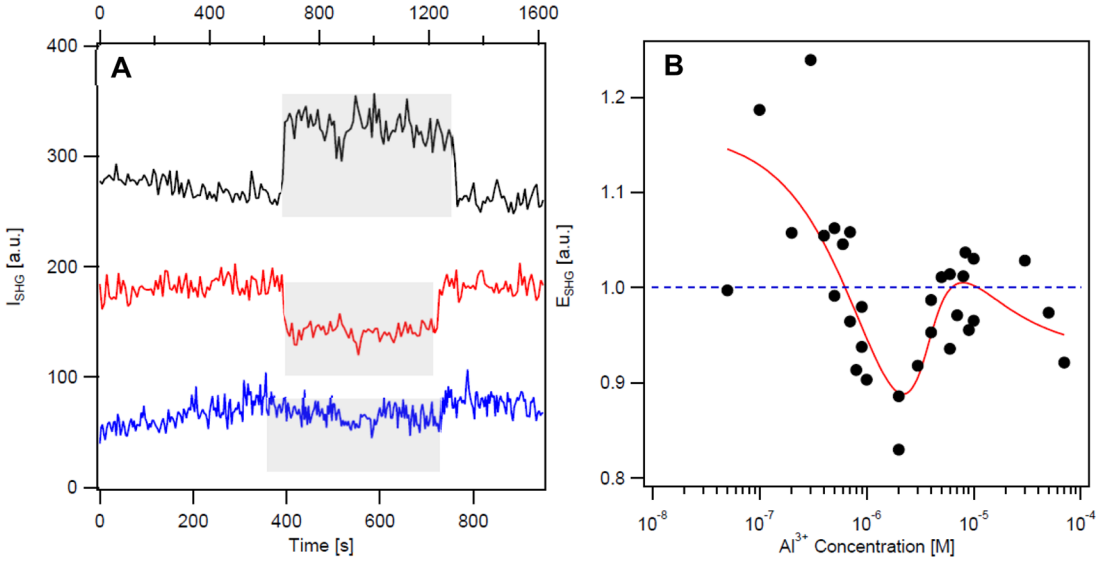

Figure 3. (A) On−off traces for 0.3 (black, bottom axis), 2 (red, bottom axis), and 10 μM (blue, top axis) Al(III). Gray shaded regions highlight the duration of time Al(III) was being flowed across the mica surface. (B) E_{SHG} as a function of a Al(III) concentration; flow rate 0.8−1 mL/sec. The red line is a guide to the eye, and the blue dashed line is the background electrolyte baseline established at the beginning of the experiment. This baseline serves as a reference for the initial interfacial potential of the mica surface. This isotherm is the combined result of three replicate experiments.

La(III) and Sc(III) atom % values suggests the presence of a competitive, dynamic environment at the muscovite surface when exposed to both La(III) and Sc(III) species. While it is apparent that Sc(III) adsorbs more readily than La(III), further investigation is required to identify trends in the chemical composition of the deposits formed as a function of exposure time, which is outside of the scope of our current study.

D. Adsorption of Aluminum. Aluminum is predicted to interact differently with mica, compared to La(III) and Sc(III), as Al(III) is already present in the tetrahedral layer comprising the mica basal surface and because it is a much harder ion than La(III) and Sc(III). Examples of the observed SHG signal intensity versus time traces that we obtained for the Al(III)/muscovite interface are shown in Figure 3A. The full adsorption isotherm, compiled from three replicate isotherm measurements, is shown in Figure 3B. We observe an initial increase in E_{SHG} at low Al(III) concentrations, then a decrease in the SHG response at intermediate Al(III) concentrations, and then a net zero change at high Al(III) concentrations when compared to the zero Al(III) concentration condition. We hypothesize that these variations in E_{SHG} are due to the formation of a secondary mineral on the mica surface, most likely gibbsite, as we elucidate below.

The secondary mineral formation of gibbsite on mica has been observed previously by Nagy et al. with tapping mode AFM and by Hanchar et al. using powder X-ray diffraction.[2,16] Gibbsite, a dioctahedral Al hydroxide, has a sheet-like structure very similar to the muscovite basal plane, making the epitaxial growth of gibbsite plausible. Natural gibbsite has a fixed surface charge density of −9.65 mC m^{-2} due to Fe^{2+} and Mg^{2+} substitutions into the octahedral layer, similar to the substitution of Al^{3+} for Si^{4+} in muscovite; however, at pH 4 and at an ionic strength of 10 mM, the surface charge density of gibbsite was calculated to be approximately +0.011 Cm^{-2}.[40] The point of zero charge (pzc) for gibbsite ranges from pH 7.8 to 10,[41] with an average pzc of pH 9; therefore, it is expected that under the experimental conditions used in our study, the available surface charge of the gibbsite deposits, if it is indeed forming on the surface, is net positive. With this information, we can further explain Figure 3B as follows: the initial increase in E_{SHG} observed when the muscovite surface is exposed to 0.1−0.3 μM Al(III) suggests that the available surface charge density becomes more negative, possibly due to the release of Al(III) ions from the exposed tetrahedral layer, a process that is facilitated by the presence of Al(III) species in solution, as reported by previous mica dissolution studies.[42−44] Any newly formed adsorption sites should be screened during the addition of Na^+, hydronium ions, or Al^{3+} or $Al(OH)^{2+}$ ions.

At approximately 0.5 μM Al(III), a decrease in the SHG response is observed, and the background signal intensity does not fully recover after the mica surface is flushed with the background electrolyte solution (data not shown), suggesting partially irreversible interactions similar to what was observed with La(III) (vide supra). We attribute this observation to the onset of gibbsite formations on the mica surface that contribute their own positive interfacial potential to the slightly negative interfacial potential of the original muscovite surface. This effect appears to be maximal when the SHG minimum is reached at an Al(III) concentration of 2 μM.

The increase in the SHG response beyond 2 μM Al(III) is attributed to the continued buildup of gibbsite deposits, which are assumed to have a net positive charge under the experimental conditions. The final slight decrease in the SHG response at high Al(III) concentrations may be due to charge screening, precipitation, and dissolution processes on the newly formed gibbsite surface, if it were indeed to form, which we expect would cause continued fluctuations in the interfacial potential as these three processes compete.

The SHG responses summarized in Figure 3B for an Al(III) flow rate of 0.8−1 mL/s differed from those observed for flow rates of 0.4−0.6 and 1.3−1.5 mL/s (Supporting Information) and would suggest that the growth of gibbsite on the surface of mica is sensitive to flow conditions in our experimental setup. Elucidation of the kinetics is beyond the scope of this work, but details regarding the flow rate dependence of Al(III) adsorbing to mica may be found in the Supporting Information.

dx.doi.org/10.1021/jp506283y | J. Phys. Chem. A 2014, 118, 10974−10981

4. CONCLUSIONS

The results presented here provide molecular insight into the interactions of three trivalent metals, namely, Al(III) and the REEs La(III) and Sc(III), at the mica−water interface. Specifically, as established herein, new dynamic and chemical information regarding the precipitation and growth of trivalent hydroxides/oxides on the mica surface is obtained. The most important environmental implication of our findings is that the value and sign (positive/negative) of the muscovite surface charge density may change when Al(III), Sc(III), or La(III) are present in solution, even at subsaturation conditions, as a result of hydroxide/oxide formation. These deposits introduce a degree of amphoterism into the system that could have a direct effect on ion−mineral interactions. By demonstrating the ability to probe the growth of amphoteric oxides directly at the mica−aqueous interface, we have in principle opened the possibility to elucidate the chemical properties and the kinetics of these precipitation processes that might otherwise go undetected. The precipitation of trivalent ions and the sensitivity of this process to pH, flow rate, and concentration of metal ions in solution, as shown in this work, illustrate the importance of this process in geochemical environments containing trivalent metals. Further investigations into the role of electrolyte concentration, pH, and exposure time are clearly needed to fully understand, control, and predict the extent of metal ion precipitation on the surfaces of mica-class minerals. Such measurements would provide the necessary information required to model how dynamic changes in the surface charge density of mineral−water interfaces may impact trivalent metal transport through heterogeneous geochemical media.

■ ASSOCIATED CONTENT

Ⓢ Supporting Information

A complete description for determining the muscovite surface charge density is provided in addition to Raman and GIAXRD spectra, SEM/EDS results for all samples analyzed, additional XPS spectra and peak positions. Details regarding Al(III) adsorption dependence on flow rate, La(III) adsorption studies at micromolar concentrations, metal speciation predictions, and SHG signal fluctuations in the absence of the 10 mM NaCl ring are also included. This material is available free of charge via the Internet at http://pubs.acs.org.

■ AUTHOR INFORMATION

Corresponding Author

*E-mail: geigerf@chem.northwestern.edu.

Notes

The authors declare no competing financial interest.

■ ACKNOWLEDGMENTS

S.A.S.G. gratefully acknowledges support from a National Science Foundation Graduate Research Fellowship. We thank Spectra-Physics Lasers, a division of Newport Corporation, for equipment support. This work made use of the J. B. Cohen X-ray Diffraction Facility supported by the MRSEC program of the National Science Foundation (DMR-1121262) at the Materials Research Center of Northwestern University. XPS, Raman, and SEM work were performed in the Keck-II facility and the EPIC facility of the NUANCE Center at Northwestern University. The NUANCE Center is supported by NSF_NSEC, NSF-MRSEC, the Keck Foundation, the State of Illinois, and Northwestern University. Support from the Environmental Chemical Sciences Program of the Division of Chemistry of the NSF under Grant # 0950433 is gratefully acknowledged.

■ REFERENCES

(1) Hochella, M. F. J.; White, A. F. Mineral−Water Interface Geochemistry. *Rev. Mineral.* **1990**, *23*, 1−16.

(2) Nagy, K. L.; Cygan, R. T.; Hanchar, J. M.; Sturchio, N. C. Gibbsite Growth Kinetics on Gibbsite, Kaolinite, and Muscovite Substrates: Atomic Force Microscopy Evidence for Epitaxy and an Assessment of Reactive Surface Area. *Geochim. Cosmochim. Acta* **1999**, *63*, 2337−2351.

(3) Geiger, F. M. Invited Article: Second Harmonic Generation, Sum Frequency Generation, and χ^3: Dissecting Environmental Interfaces with a Nonlinear Optical Swiss Army Knife. *Annu. Rev. Phys. Chem.* **2009**, *60*, 61−83.

(4) Morel, F. M. M.; Hering, J. G. *Principles and Applications of Aquatic Chemistry*; John Wiley & Sons, Inc.: New York, 1993.

(5) Stumm, W.; Morgan, J. J. *Aquatic Chemistry: Chemical Equilibria and Rates in Natural Waters*, 3rd ed.; Wiley: New York, 1996.

(6) Schlegel, M. L.; Nagy, K. L.; Fenter, P.; Cheng, L.; Sturchio, N. C.; Jacobsen, S. D. Cation Sorption on the Muscovite (0 0 1) Surface in Chloride Solutions Using High-Resolution X-ray Reflectivity. *Geochim. Cosmochim. Acta* **2006**, *70*, 3549−3565.

(7) Tan, K. H. *Environmental Soil Science*, 2nd ed.; Marcel Dekker, Inc.: New York, 2000.

(8) Chakraborty, S.; Wolthers, M.; Chatterjee, D.; Charlet, L. Adsorption of Arsenite and Arsenate onto Muscovite and Biotite Mica. *J. Colloid Interface Sci.* **2007**, *309*, 392−401.

(9) Klien, C.; Dutrow, B.; Dana, J. D. *The 23rd ed. of the Manual of Mineral Science*, 23 ed.; John Wiley & Sons, Inc.: Hoboken, NJ, 2008.

(10) Loewenstein, W. The Distribution of Aluminum in the Tetrahedra of Silicates and Aluminates. *Am. Mineral.* **1954**, *39*, 92−96.

(11) Humphries, M. In *Rare Earth Elements: The Global Supply Chain*; Service, C. R., Ed.; Congressional Research Service: Washington, DC, 2012.

(12) Kagan, H. B. Introduction: Frontiers in Lanthanide Chemistry. *Chem. Rev.* **2002**, *102*, 1805−1806.

(13) Weber, R. J.; Reisman, D. J. In *Rare Earth Elements: A Review of Production, Processing, Recycling, and Associated Environmental Issues*; Agency, U. E. P., Ed.; U.S. Environmental Protection Agency: Kansas City, KS, 2012.

(14) Folger, T. *The Secret Ingredients of Everything*; National Geographic: Washington, DC, 2011; p 136−145.

(15) Haxel, G. B.; Hedrick, J. B.; Orris, G. J. *Rare Earth Elements - Critical Resources for High Technology*; U.S. Geological Survey: Reston, VA, 2002.

(16) Hanchar, J. M.; Nagy, K. L.; Fenter, P.; Finch, R. J.; Beno, D. J.; Sturchio, N. C. Quantification of Minor Phases in Growth Kinetics Experiments with Powder X-ray Diffraction. *Am. Mineral.* **2000**, *85*, 1217−1222.

(17) Knauss, K. G.; Thomas, J. W. Muscovite Dissolution Kinetics as a Function of pH and Time at 70°C. *Geochim. Cosmochim. Acta* **1989**, *53*, 1493−1501.

(18) Sunding, M. F.; Hadidi, K.; Diplas, S.; Løvvik, O. M.; Norby, T. E.; Gunnæs, A. E. XPS Characterisation of in Situ Treated Lanthanum Oxide and Hydroxide Using Tailored Charge Referencing and Peak Fitting Procedures. *J. Electron Spectrosc. Relat. Phenom.* **2011**, *184*, 399−409.

(19) Biesinger, M. C.; Lau, L. W. M.; Gerson, A. R.; Smart, R. S. C. Resolving Surface Chemical States in XPS Analysis of First Row Transition Metals, Oxides and Hydroxides: Sc, Ti, V, Cu and Zn. *Appl. Surf. Sci.* **2010**, *257*, 887−898.

(20) Waite, T. D.; Davis, J. A.; Payne, T. E.; Waychunas, G. A.; Xu, N. Uranium(Vi) Adsorption to Ferrihydrite: Application of a Surface Complexation Model. *Geochim. Cosmochim. Acta* **1994**, *58*, 5465−5478.

(21) Cygan, R. T.; Greathouse, J. A.; Heinz, H.; Kalinichev, A. G. Molecular Models and Simulations of Layered Materials. *J. Mater. Chem.* **2009**, *19*, 2470−2481.
(22) Saslow Gomez, S.; Jordan, D. S.; Troiano, J.; Geiger, F. M. Uranyl Adsorption at the Muscovite (Mica)/Water Interface Studied by Second Harmonic Generation. *Environ. Sci. Technol.* **2012**, *46*, 11154−11161.
(23) Hayes, P. H.; Malin, J. N.; Konek, C. T.; Geiger, F. M. Interaction of Nitrate, Barium, Strontium and Cadmium Ions with Fused Quartz/Water Interfaces Studied by Second Harmonic Generation. *J. Phys. Chem. A* **2008**, *112*, 660−668.
(24) Malin, J. N.; Hayes, P. L.; Geiger, F. M. Interactions of Ca, Zn, and Cd Ions at Buried Solid/Water Interfaces Studied by Second Harmonic Generation. *J. Phys. Chem. C* **2008**, *113*, 2041−2052.
(25) Mifflin, A. L.; Musorrafiti, M. J.; Konek, C. T.; Geiger, F. M. Second Harmonic Generation Phase Measurements of Cr(VI) at a Buried Interface. *J. Phys. Chem. B* **2005**, *109*, 24386−24390.
(26) Al-Abadleh, H. A.; Mifflin, A. L.; Musorrafiti, M. J.; Geiger, F. M. Kinetic Studies of Chromium (VI) Binding to Carboxylic Acid- and Methyl Ester-Functionalized Silica/Water Interfaces Important in Geochemistry. *J. Phys. Chem. B* **2005**, *109*, 16852−16859.
(27) Hayes, P. H.; Gibbs-Davis, J. M.; Musorrafiti, M. J.; Mifflin, A. L.; Scheidt, K. A.; Geiger, F. M. Environmental Biogeochemistry Studied by Second-Harmonic Generation: A Look at the Agricultural Antibiotic Oxytetracycline. *J. Phys. Chem. C* **2007**, *111*, 8796.
(28) Gibbs-Davis, J. M.; Kruk, J. J.; Konek, C. T.; Scheidt, K. A.; Geiger, F. M. Jammed Acid−Base Chemistry at Interfaces. *J. Am. Chem. Soc.* **2008**, *130*, 15444−15447.
(29) Mifflin, A. L.; Gerth, K. A.; Geiger, F. M. Kinetics of Chromate Adsorption and Desorption at Fused Quartz/Water Interfaces Studied by Second Harmonic Generation. *J. Phys. Chem. A* **2003**, *107*, 9620−9627.
(30) Eisenthal, K. B. Liquid Interfaces Probed by Second-Harmonic and Sum-Frequency Spectroscopy. *Chem. Rev.* **1996**, *96*, 1343.
(31) Ong, S.; Zhao, X.; Eisenthal, K. B. Polarization of Water Molecules at a Charged Interface: Second Harmonic Studies of the Silica/Water Interface. *Chem. Phys. Lett.* **1992**, *191*, 327.
(32) Hayes, P. L.; Chen, E. H.; Achtyl, J. A.; Geiger, F. M. An Optical Voltmeter for Studying Cetyltrimethylammonium Interacting with Fused Silica/Aqueous Interfaces at High Ionic Strength. *J. Phys. Chem. A* **2009**, *113*, 4269−4280.
(33) Hayes, P. L.; Malin, J. N.; Jordan, D. S.; Geiger, F. M. Get Charged Up: Nonlinear Optical Voltammetry for Quantifying the Thermodynamics and Electrostatics of Metal Cations at Aqueous/Oxide Interfaces. *Chem. Phys. Lett.* **2010**, *499*, 183−192.
(34) Langmuir, D. *Aqueous Environmental Geochemistry*; Prentice Hall, Inc.: Upper Saddle River, NJ, 1997.
(35) Jena, K. C.; Covert, P. A.; Hore, D. K. The Effect of Salt on the Water Structure at a Charged Solid Surface: Differentiating Second- and Third-Order Nonlinear Contributions. *J. Phys. Lett.* **2011**, *2*, 1056−1061.
(36) Teich-McGoldrick, S. L.; Greathouse, J. A.; Cygan, R. T. Molecular Dynamics Simulations of Uranyl Adsorption and Structure on the Basal Surface of Muscovite. *Mol. Simul.* **2014**, *40*, 610−617.
(37) Jordan, D. S.; Saslow, S. A.; Geiger, F. M. Exponential Sensitivity and Speciation of Al(III), Sc(III), Y(III), La(III), and Gd(III) at Fused Silica/Water Interfaces. *J. Phys. Chem. A* **2011**, *115*, 14438−14445.
(38) Troiano, J. M.; Jordan, D. S.; Hull, C. J.; Geiger, F. M. Interaction of Cr(III) and Cr(VI) with Hematite Studied by Second Harmonic Generation. *J. Phys. Chem. C* **2013**, *117*, 5164−5171.
(39) Seitz, M.; Oliver, A. G.; Raympnd, K. N. The Lanthanide Contraction Revisited. *J. Am. Chem. Soc.* **2007**, *129*, 11153−11160.
(40) Kraepiel, A. M. L.; Keller, K.; Morel, F. M. M. On the Acid−Base Chemistry of Permanently Charged Minerals. *Environ. Sci. Technol.* **1998**, *32*, 2829−2838.
(41) Karamalidis, A. K.; Dzombak, D. A. *Surface Complexation Modeling: Gibbsite*; Wiley: New York, 2010.
(42) Pachana, K.; Zuddas, P.; Censi, P. Influence of pH and Temperature on the Early Stage of Mica Alteration. *Appl. Geochem.* **2012**, *27*, 1738−1744.
(43) Oelkers, E. H.; Schott, J.; Gauthier, J.-M.; Herrero-Roncal, T. An Experimental Study of the Dissolution Mechanism and Rates of Muscovite. *Geochim. Cosmochim. Acta* **2008**, *72*, 4948−4961.
(44) Gérard, F.; Fritz, B.; Clément, A.; Crovisier, J.-L. General Implications of Aluminium Speciation-Dependent Kinetic Dissolution Rate Law in Water−Rock Modelling. *Chem. Geol.* **1998**, *151*, 247−258.